Numerical and Experimental Investigation of the Effects of Thin Hard Coatings on the Strength of Spur Gears

Sergio Baragetti*

Department of Management, Information and Production Engineering, University of Bergamo, Viale Marconi 5, 24044 Dalmine (BG), Italy

Abstract: The use of thin films to coat mechanical components is a well-established practice. The main uses concern areas in which scratch resistance, corrosion resistance, surface hardness and particular aesthetic characteristics are required. In addition to these properties, it has been demonstrated that Physical Vapor Deposition (PVD) processes bring further benefits from a structural point of view, especially as regards fatigue and contact fatigue phenomena. In this research work, predictive models have been proposed which allow to evaluate the mechanical behavior of coated components to model the initiation and propagation of cracks. Spur gears used in the automotive and motorcycle industries were examined. Therefore, advanced numerical models were developed to accurately evaluate the stress-strain state of the components under examination, both as regards the fatigue at the tooth base and for the contact fatigue on the tooth flank. The results of the numerical models were finally compared with the results of the experimental tests to verify their accuracy.

Keywords: Spur gears, PVD coating, Fatigue, FEM models, Experimental procedures, Automotive and motorcycle applications.

1. INTRODUCTION

Thin film deposition techniques enable the application, on the surface of a component, of an extremely hard material layer having a thickness of more than a few μm. The methods for obtaining these coatings are based on processes that take place under vacuum. The main ones are thermal evaporation, electron beam evaporation and sputtering. With these techniques, phase transformations of the material with which the coating layer is to be made are carried out: the starting material, in solid form, must be vaporized and subsequently condensed on a substrate, thus forming the thin film. Deposition processes of this type are collectively labeled as Physical Vapor Deposition (PVD) and are distinct from Chemical Vapor Deposition (CVD) processes, in which chemical reactions both in the gaseous phase and on the substrate surface play a fundamental role. Through these processes it is possible to create thin films of the most diverse materials for different applications, from the less sophisticated ones (coating of costume jewelry and trophies, coating of razor blade edges, decorative sheets, coating of samples for electron microscopy) to the more sophisticated ones (layers used in microelectronics, ohmic contacts, resistors and conductors, high performance optical components, protective coatings, mirrored sunglasses, etc.). PVD coatings are widely used in the world of competitions, for example in motorcycling forks they are used with stems coated with titanium nitride (TiN) or aluminum titanium nitride (AlTiN), which considerably increase the surface hardness, and therefore the wear resistance, of the steel tube of the fork stem itself. TiN coatings are also used on other parts subject to wear such as titanium connecting rod heads and valve stems. The most widespread technique for coating hard materials, such as titanium nitride (TiN), titanium carbonitride (TiCN), aluminum titanium nitride (AlTiN), chromium nitride (CrN) and zirconium nitride (ZrN) is PVD. CVD and PVD hard thin film deposition techniques are popular in many mechanical applications. The coatings obtained provide excellent performance in terms of wear resistance, hardness and corrosion resistance [1-5]. Furthermore, the residual stresses generated by the deposition processes in the surface layer of the coated components contribute to alter their fatigue limit [6-11], an aspect that can be further investigated and on which the research work has focused.

The objective of this paper is to study, through finite element models (FEM) and subsequent experimental tests, the behavior of a CrN coating (Figure **1**), from the point of view of fatigue and contact fatigue resistance, applied to spur gears of mechanical transmissions both for motorcycle racing and automotive industries. In particular, the pinion - fifth gear pair (hardened 16NiCr11) of a racing motorcycle and the reverse spur

*Address correspondence to this author at the Department of Management, Information and Production Engineering, University of Bergamo, Viale Marconi 5, 24044 Dalmine (BG), Italy;
E-mail: sergio.baragetti@unibg.it

E-ISSN: 2410-4701/22

gear (hardened 18NiCrMo5) of a medium-large car engine were examined. For the motorcycle gears, FEM models were created, simulating the matching between the pinion and the driven gear, to investigate the fatigue phenomena at the base of the tooth, comparing untreated, case-hardened and coated steel gears; the fatigue behavior of a gear made of coated titanium alloy (Ti6Al4V), a material that provides, as other light alloys, a significant mass saving compared to steel [12, 13], was also evaluated. The mechanical properties of the mentioned materials are reported in Table **1**. Experimental static and fatigue tests were carried out on the automotive-type gear, and FEM models were created that simulated the test conditions so as to be able to compare the numerical models with the experimental results. The test system involves forcing a cylinder (100Cr6 hardened on the surface), with a diameter of 8 mm and a length of 20 mm, between two successive teeth. In this way the cylinder-teeth contact takes place in the outermost point of contact, which is the most critical from the point of view of the load on the tooth, during the transmission of motion between a pair of gears.

Figure 1: CrN layer applied on a steel substrate.

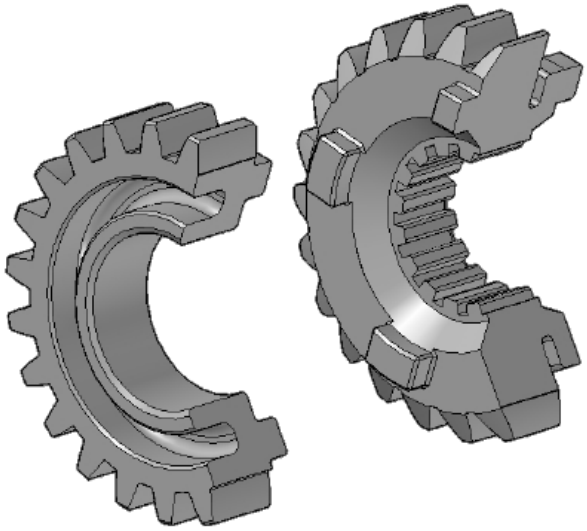

Figure 2: 3D models of the spur gears.

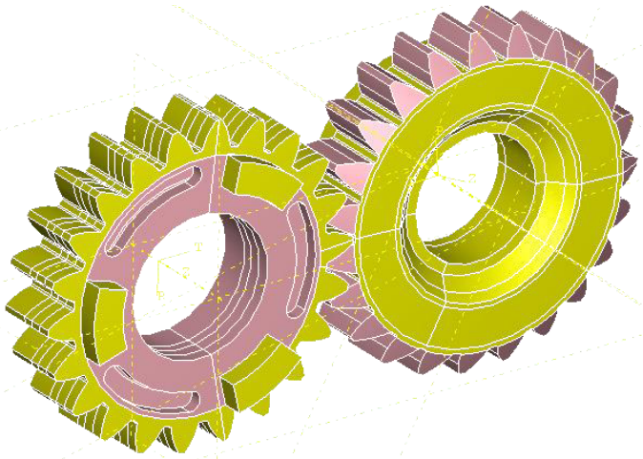

Figure 3: 3D model of the matching spur gears.

2. NUMERICAL FEM MODELS

The FEM simulations were carried out with the aid of the commercial software ABAQUS [14], with which it is possible to effectively model critical conditions such as the contact between the tooth flanks, the presence of the thin ceramic coating, the presence of a surface

Table 1: Mechanical Properties of the Materials

	E [MPa]	ν	Ys [MPa]	Rm [MPa]	HV
CrN	306000	0.2		3000	1750
16NiCr11	206000	0.3	1100	1350	757
18NiCrMo5	206000	0.3	690	828	556
100Cr6	206000	0.3	1650	1900	848
Ti6Al4V	110000	0.34	880	950	349

defect and the residual stresses induced by the PVD treatment. The geometry of the gears supplied by Ducati Corse, devoid of symmetries due to the presence of lightening (Figure **2**), does not allow for simplifications. A complete three-dimensional model of the matching spur gears was then created (Figure **3**) with elements of the solid type (elements of the type C3D8 with linear shape function [14]). In this phase, particular attention was paid to the imposition of constraints, loads and contact interaction between the flanks of the matching teeth. In particular, the driven gear was constrained by means of a joint which blocks all its degrees of freedom, while the pinion was left free to rotate on its own axis so as to be able to transmit the necessary torque. The latter was simulated, for simplicity, by applying a force concentrated on the pinion tooth opposite to the one that comes into contact with the driven gear. This setting is not physically correct, since it does not represent the actual condition of transmission of the engine torque, which actually takes place through the axial engagement. However, the simplification introduced has no influence on the stress-strain state at the base of the tooth to be analyzed.

Since it is too expensive, from a computational point of view, to simultaneously simulate the matching between the gears, the presence of a crack and the residual stresses due to the PVD process, it was chosen to divide the problem into two parts. With an assembly model (global model) the forces that the gears exchange at a macroscopic level were simulated, without considering the presence of the crack. The mesh was then refined on the teeth that come into contact and the coating was simulated in a simplified way with 5-point shell elements [14]. Subsequently, a smaller model (submodel) was created, which takes into consideration only the most stressed area at the base of the tooth of the driven gear, including the crack, residual stresses and surface coating (Figure **4**). The nodal displacements resulting from the simulations on the global model were transferred to this model. Since fatigue failure often occurs due to surface defects, semi-elliptical surface cracks were simulated (Figure **4**). To impose the residual stresses due to the coating deposition process, the submodel was divided into cells, each with a thickness of 5 μm, on which a suitable temperature profile was applied, necessary to induce the desired residual stress field (Figure **5**). In this phase of residual stress modelling the submodel was constrained with trolleys limiting the degrees of freedom in all directions. In the next step the boundary conditions coming from the global model were applied,

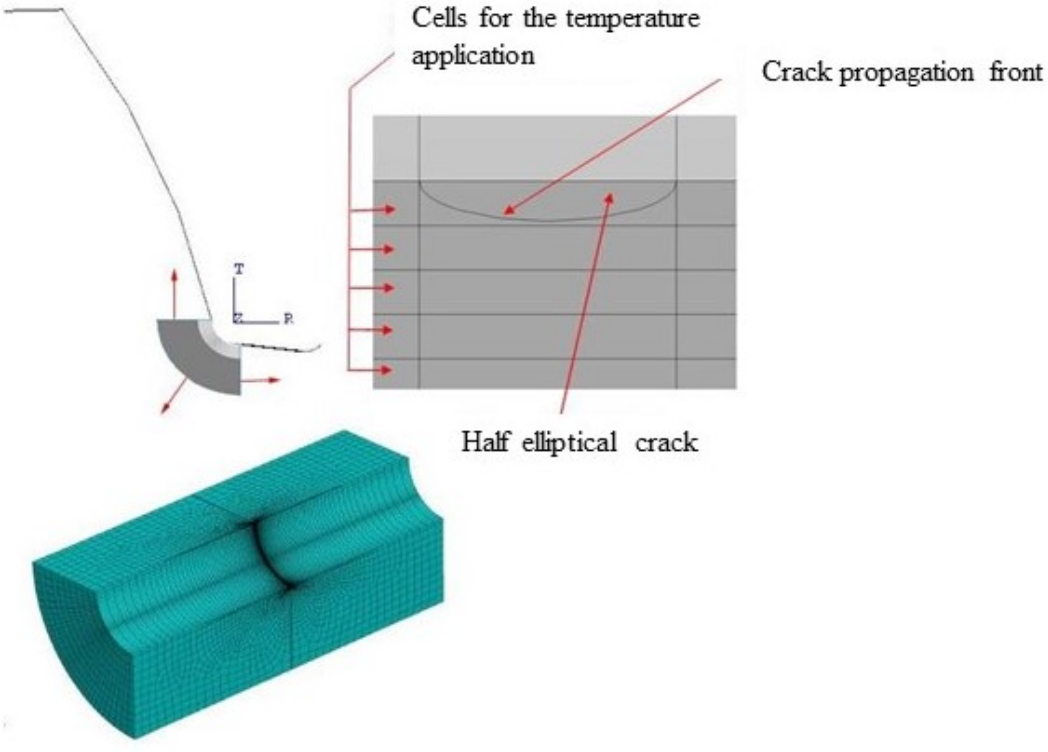

Figure 4: Submodel of the area at the root of the teeth of the spur gears.

the constraints previously imposed on the submodel were deactivated. To avoid that during the load cycle the two faces of the crack interpenetrate, due to the state of compression induced, it was necessary to impose a contact constraint on them (self-contact). Simulations were carried out for models of steel and titanium gears, with and without coating, with crack depths of 5, 25, 50, 100, 200, 400 μm, respectively. The generation of the cracks took place through a dedicated function of Abaqus, which allows to draw the shape and the arrangement plane. For each crack, a submodel was created in which the mesh was controlled, since these are extremely limited areas with a strong stress gradient. For all models, the behavior of the material, both for the coating and for the substrate, was considered linear elastic. This is because the analytical forecasting models to be used refer to the propagation of cracks in the elastic field.

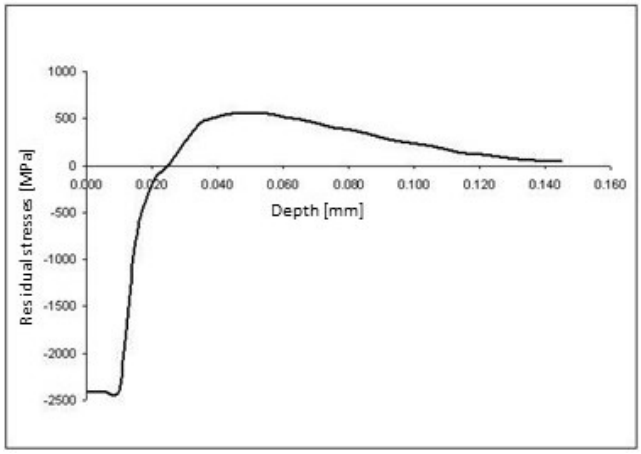

Figure 5: Trend of residual stresses due to the PVD process.

On automotive spur gears, the action of the cylinder is simulated which, due to the imposed vertical load, is forced between two neighboring teeth. Given the greater simplicity of the gear compared to the previous

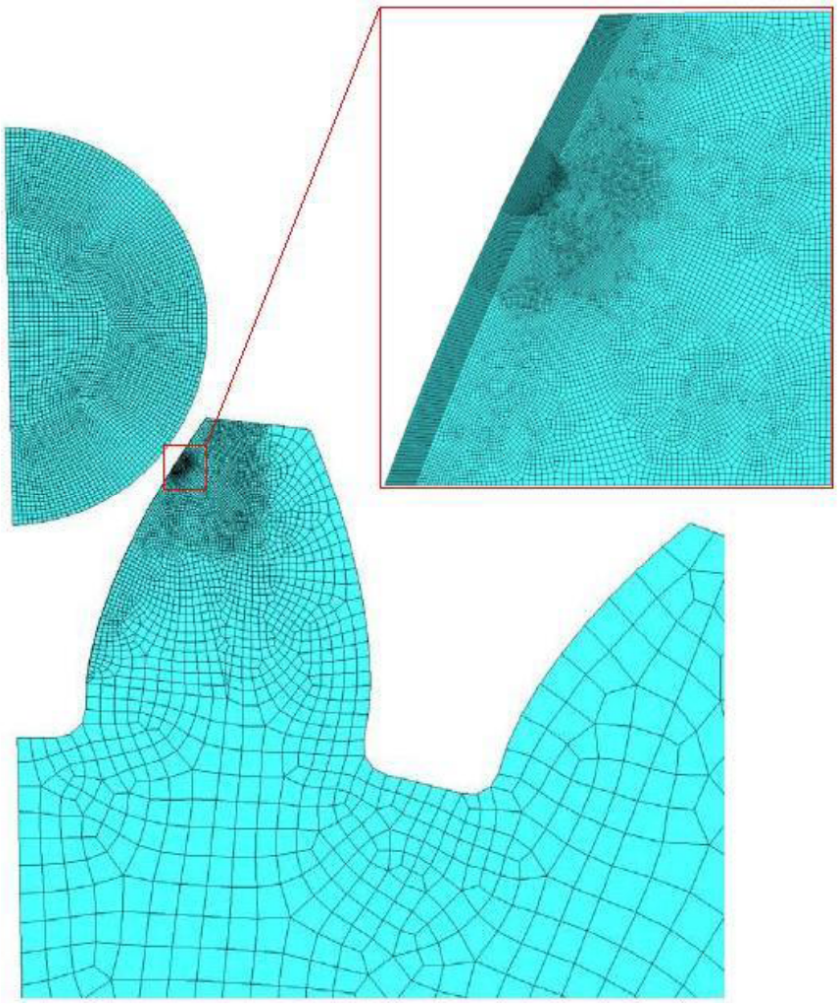

Figure 6: Mesh of the global model and of the submodel for automotive spur gears.

ones and the symmetry of the problem, it is possible to create a 2D model (elements of the type CPS4 with a linear shape function [14]) of half the gear, taking care to set the appropriate symmetry constraints. As seen previously, the problem was tackled using two different models (Figure **6**), a global one with which the cylinder-gear contact was simulated on a macroscopic scale, taking care to operate a refinement of the mesh in the contact area in which the results in terms of stresses and deformations must be accurate, and a submodel which refined the analysis in the contact area and with which the surface coating and the presence of residual stresses were accurately modeled. Through the submodel it was possible to accurately obtain the stress and strain values both in the coating and in the substrate in the contact area. To adequately simulate the real mechanical behavior of the components studied, both the steel of the gear and that of the stressing cylinder were considered to have an elastic-plastic behavior, reconstructing the stress-strain curve from literature data (Figure **7**); the coating material, on the other hand, was considered purely elastic given its substantially fragile nature. Considering the elastic-plastic behavior is fundamental in these simulations, given that the area of interest is the contact area in which, given the high loads involved, localized plastic deformations can be expected to occur.

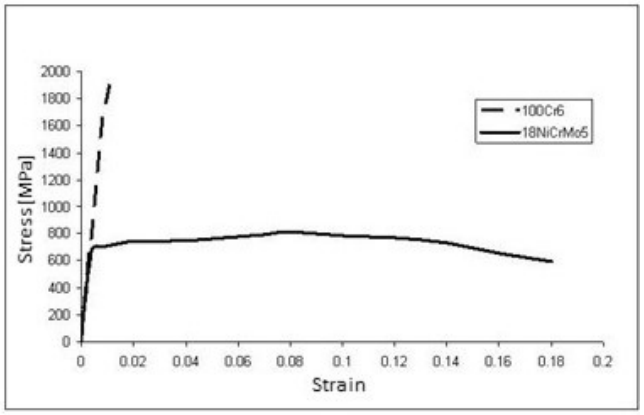

Figure 7: Stress-strain curve for 18NiCrMo5 and 100Cr6 steels.

3. RESULTS

As regards the spur gears supplied by Ducati Corse, the contact pressure on the tooth was obtained from the global model, which was not symmetrical along the depth due to the different geometry of the pinion and driven gear teeth (Figure **8**). The stress and strain values at the crack tip were obtained from the submodel (Figures **9-10**) and the opening of the various cracks was measured (Figure **11**), a parameter which, through appropriate theoretical models, makes it possible to establish whether the crack is advancing,

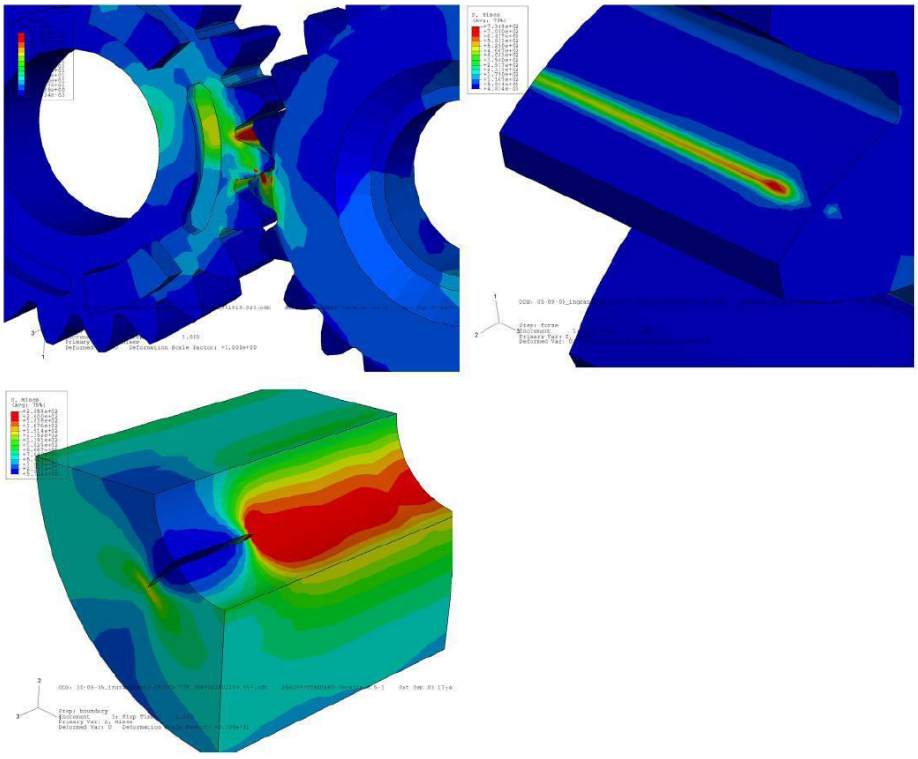

Figure 8: Von Mises stress map for the global model and the submodel.

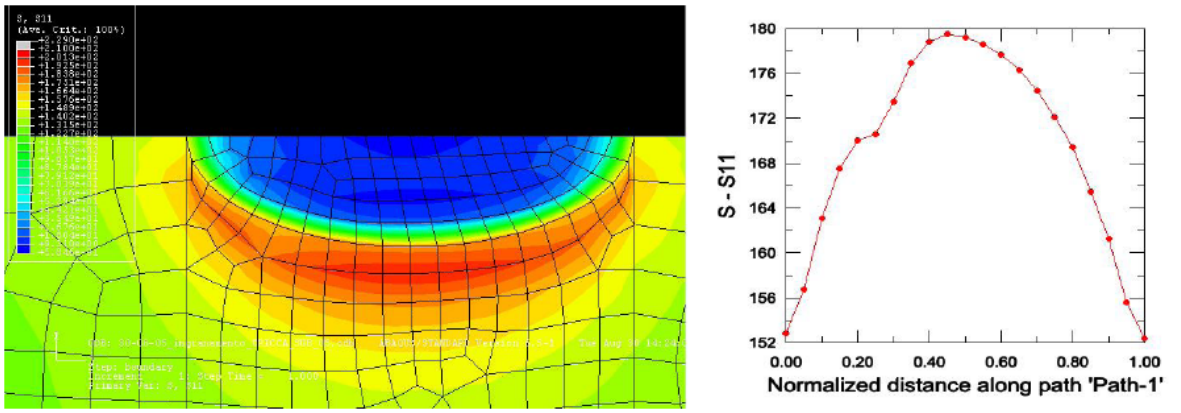

Figure 9: Maximum principal stress at the crack tip, uncoated model.

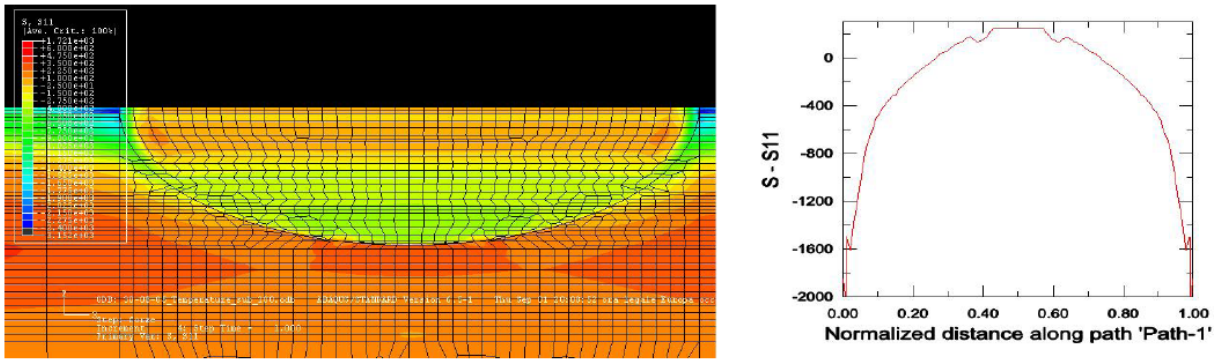

Figure 10: Maximum principal stress at the crack tip, coated model.

the feed rate and the number of load cycles for which the crack depth is critical to the component strength (unstable crack propagation).

The simulations carried out show that the deposition of the coating and the applied residual stresses greatly influence the stress state at the crack tip; in fact, the state of compression on the surface of the component and in the immediately underlying layers, induced by the deposition process, tends to close the crack, as opposed to the bending due to the load on the tooth, which instead tends to open it.

3.1. Calculation of the Stress Intensity Factor

To evaluate the criticality of the defect, it is necessary to determine the stress intensity factor (K_I) and compare it with a theoretical threshold value which indicates the limit beyond which there is unstable propagation of the defect. For the analytical calculation of K_I, the definition of "c-open" [15] was used, which involves calculating the stress intensity factor based on the relative semi-displacement between the two faces of the crack (Figure **11**) according to the formula 1:

$$1\ K_I = \frac{2E}{1+\upsilon}\frac{u}{f(\theta)}\sqrt{\frac{2\pi}{r}} \tag{1}$$

With:

$$f(\theta) = \sin\left(\frac{\theta}{2}\right)\left[(\chi+1) - 2\cos^2\left(\frac{\theta}{2}\right)\right]$$

Where:

$\chi = \frac{3-\upsilon}{1+\upsilon}$: for plane strain

$\chi = 3-4\upsilon$: for plane stress

And having defined:

- υ : Poisson's ratio;
- r: distance, in polar coordinates, between the crack tip and the point considered;
- θ : opening angle.

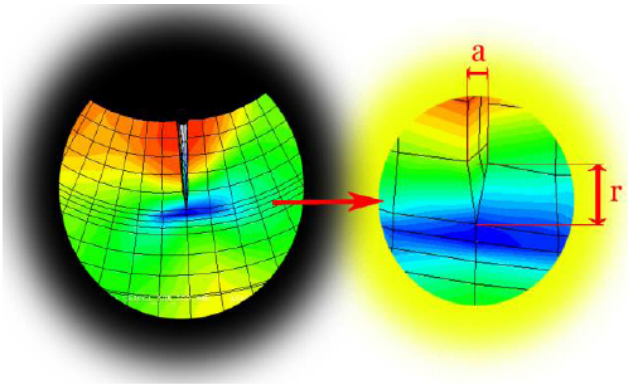

Figure 11: Crack tip and definition of the geometric parameters.

To establish whether the crack is advancing, it is necessary to compare the K_I thus determined with a threshold value evaluated using the most appropriate theoretical model. The choice of the threshold intensification factor must be made according to two parameters:

a : crack length;

a_0: El-Haddad parameter [16, 17], defined by formula 2:

$$a_0 = \left(\frac{\Delta K_{th,Ic}}{\beta \Delta \sigma_{wo}} \right)^2 \frac{1}{\pi} \tag{2}$$

Where:

$\Delta K_{th,Ic}$ is the threshold stress intensity factor range determinable with the experimental formula elaborated by Masana Kato, Gang Deng, Katsumi Inoue, Enobou Takatsu [18]:

$$\Delta K_{th,Ic} = 2.45 + 3.41 \cdot 10^{-3} H$$

Determination of *H* needs the following parameters:

- H_1 : surface Vickers hardness;
- H_2 : maximum Vickers hardness;
- H_3 : core Vickers hardness;
- H_4 : coating-substrate limit Vickers hardness;
- d_2 : depth at which the hardness reaches its maximum value;
- d_{eff} : effective depth of the protective surface layer;

$$H = (H_2 - H_3) e^{-A(d_{eff} - d_2)^2 + H_3}$$

$$A = -\frac{1}{d_2^2} ln\left(\frac{H_1 - H_3}{H_2 - H_3}\right) \quad d \le d_2$$

$$A = -\frac{1}{(d_{eff} - d_2^2)^2} ln\left(\frac{H_4 - H_3}{H_2 - H_3}\right) \quad d > d_2$$

- β is the shape factor derived from the inverse formula of the stress intensity factor (3):

$$K_{th} = \sigma \beta \sqrt{\pi a} \tag{3}$$

- $\Delta \sigma_{wo}$ is the fatigue limit.

a / a_0 can be taken from Table **2**:

Table 2: Fracture Mechanics Parameter a / a_0

	Model
a / a_0 ≤ 3 ÷ 5	Murakami Endo
3 < a / a_0 < 10	El Haddad
a / a_0 ≥ 10	MFLE (Linear elastic fracture mechanics)

According to Murakami Endo [19] model (formula 4):

$$\Delta K_{th} = 3.3 \cdot 10^{-3} (H + 120) \left(\sqrt{area}\right)^{1/3} \left(\frac{1 - R}{2}\right)^{\alpha} \tag{4}$$

$$\alpha = 0.226 + H \cdot 10^{-4}$$

where $\sqrt{area}$ is a geometric parameter similar to the depth of the crack.

According to El-Haddad [16, 17] model (formula 5):

$$\Delta K_{th} = \Delta K_{th,Ic} \sqrt{\frac{a}{a + a_0}} \tag{5}$$

In the third model $\Delta K_{th} = \Delta K_{th,Ic}$.

ΔK_{th} therefore depends on the hardness parameter H which varies significantly depending on whether the case-hardened steel substrate is considered or not.

3.2. Crack Propagation Models

For models in which there are propagating cracks, it is possible to estimate crack propagation rate

$\left(\frac{da}{dN}\right)$ and the number of cycles associated with it through the formulas of Kato, Deng, Inoue and Takatsu [18] (formula 6):

$$\frac{da}{dN} = \frac{C}{\left(1-\rho^n\right)}\left(\Delta K^n - \Delta K_{th}^n\right) \qquad \text{per } \Delta K_{th} \leq \Delta K \leq K_C \quad (6)$$

$$\frac{da}{dN} = \frac{C}{\left(1-\rho^n\right)}\left(\frac{\Delta K^n \Delta K_{IC}}{\Delta K_{IC} - \Delta K}\right) \qquad \text{per } K_C < \Delta K < K_{IC}$$

The parameters are formulated using experimental results and values of the crack propagation rate found in the technical literature: $\rho = \frac{\Delta K_{th}}{K_{IC}}$, with:

- $K_C = \sqrt{\Delta K_{th} K_{IC}}$
- $K_{IC} = 141 - 1.64 \cdot 10^{-1} H$
- $n = 4.31 - 8.66 \cdot 10^{-3} H + 1.17 \cdot 10^{-5} H^2$
- $log(C) = -10.0 + 1.09 \cdot 10^{-2} H - 1.40 \cdot 10^{-5} H^2$

The simulations show that, for models with not case-hardened substrates, the introduction of the coating, with the relative residual stresses, brings a considerable benefit since the state of compression caused by the latter prevents the opening of the cracks, and therefore their propagation, up to lengths of 100 μm for steel gears and 200 μm for titanium gears (Table 3). Thanks to the pretensions and the coating, if there are no defects greater than 100 μm and 200 μm respectively, there is no propagation. In the opposite case, *i.e.* in the presence of defects of greater depth, there is a maximum limit of 100000 cycles, for gears with a steel substrate, and 140000 cycles, for gears with a titanium substrate, to reach up to 400 μm. In the uncoated model, on the other hand, there is propagation already starting from 25 μm long defects. As regards the models with case-hardened substrate, there is no propagation of defects for the cracks taken into consideration, already in the model without coating; the introduction of the coating is therefore not necessary. However, it can be noted that the introduction of the coating causes the cracks not to open up to a length of 100 μm; furthermore, for cracks larger than this size, the difference between the value of the effective stress intensity factor and the threshold value is greater than the difference between the analogous parameters obtained in the uncoated model. This last aspect leads to believe that coated gears can still withstand higher load conditions, maintaining excellent fatigue behavior.

As regards the results from the simulations on automotive-type gears, the objective of the analyzes is to accurately evaluate the behavior of the contact patch in the event that there is a ceramic coating. In particular through the submodeling technique already described, it is possible to determine the state of stress and deformation in the coating and in the substrate (Figure **12**) which allows to verify the possible achievement of the critical failure conditions for the coating; once the limit load which leads to failure of the coating has been determined, by imposing gradually lower loads, it is possible to obtain the deformation values which, through an appropriate theoretical model, allow to determine the number of cycles for which the initiation of a crack occurs.

In a first analysis it is useful to compare the value of the contact pressure, obtained through the numerical model, with that calculated according to the Hertz

Table 3: Comparison among the Results in Different Conditions for Motorcycle Spur Gears

Crack depth [μm]	Untreated steel	Case-hardened steel	PVD coated steel	PVD coated Ti6Al4V
5	No crack propagation	No crack propagation	No crack propagation	No crack propagation
25	Crack propagation	No crack propagation	No crack propagation	No crack propagation
50	Crack propagation	No crack propagation	No crack propagation	No crack propagation
100	Crack propagation	No crack propagation	Crack propagation	No crack propagation
200	Crack propagation	No crack propagation	Crack propagation	Crack propagation
400	Crack propagation	No crack propagation	Crack propagation	Crack propagation
Number of cycles	100000	/	100000	140000

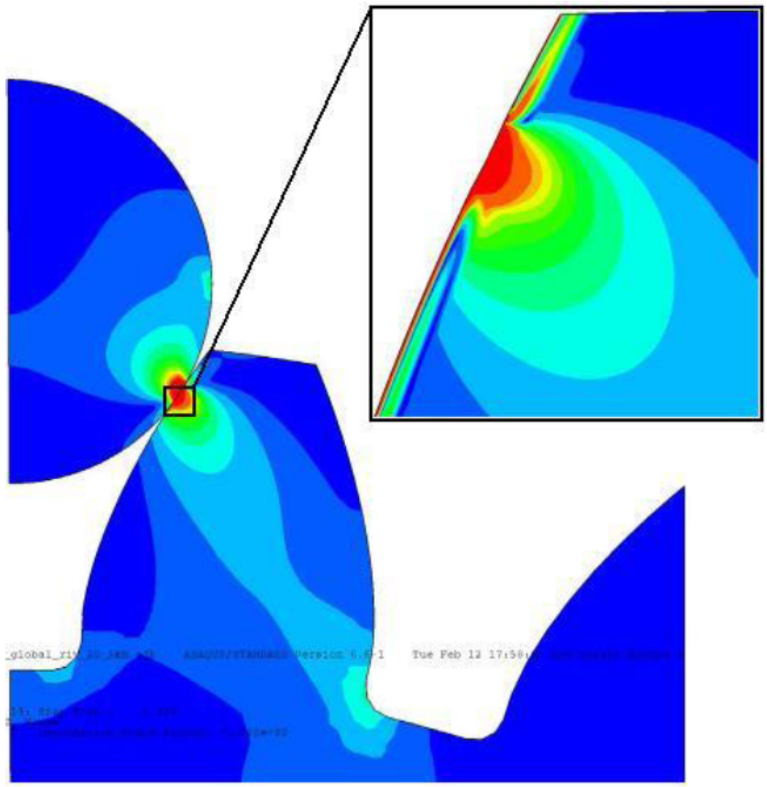

Figure 12: Von Mises stress in global model and submodel for automotive spur gears.

theory [20], which provides for determining the contact pressure between two cylinders according to the formula 7:

$$\sigma_C = \left(\frac{Wt}{\pi F \cos\varphi} \frac{\frac{1}{r_1} + \frac{1}{r_2}}{\left[\frac{(1-\nu_1^2)}{E_1}\right] + \left[\frac{(1-\nu_2^2)}{E_2}\right]} \right)^{\frac{1}{2}} \quad (7)$$

Where r_1 and r_2 are the radii of the cylinders in contact, respectively the cylinder used in the test and the osculating cylinder of the tooth at the point of contact, *Wt* is the tangential component of the load acting on the tooth, F is the thickness of the tooth, E_1, E_2 and ν_1, ν_2 are respectively the Young's modulus and the Poisson's ratio of the materials in contact. The numerical model takes into account the elastic-plastic behavior of the metal substrate, the reduced thickness of the ceramic coating and friction, parameters which are not considered in the Hertz theoretical model, but which greatly influence the contact pressures. As regards the determination of the number of cycles leading to the initiation of a crack in the contact zone, the theoretical model used is based on the Coffin-Manson (formula 8), Morrow (formula 9) and Smith-Watson-Topper (formula 10) relationships [21], which allow to link the strain due to the load on the tooth to the number of cycles necessary for the initiation of a crack.

Coffin-Manson equation: $\varepsilon_{at} = \frac{\sigma'_f}{E}\left(2N_f\right)^b + \varepsilon'_f\left(2N_f\right)^c$ (8)

Morrow approach:

$$\varepsilon_{at} = \frac{\sigma'_f}{E}\left(1 - \frac{\sigma_m}{\sigma'_f}\right)\left(2N_f\right)^b + \varepsilon'_f\left(2N_f\right)^c \quad (9)$$

Smith-Watson-Topper approach:

$$\sigma_{\max}\varepsilon_a = \sigma'_f\left(2N_f\right)^b\left[\frac{\sigma'_f}{E}\left(2N_f\right)^b + \varepsilon'_f\left(2N_f\right)^c\right] \quad (10)$$

ε_{at} is the total strain obtained from the numerical models in which the cyclic curve has been used to define the behavior of the material, N_f is the number of cycles that leads to the initiation of the crack, $\sigma'_f, \varepsilon'_f$, *b* and *c* are parameters of the material available in the literature.

From the numerical models it is therefore possible to obtain the maximum strain values (ε_a) for the applied

loads to be inserted in the theoretical models to determine the maximum number of cycles (N_f) for which a crack is initiated. The simulations were conducted for applied loads of 15 kN, 10 kN and 5 kN respectively on the coated gear; for all the simulated cases it can be seen that the stress in the coating is such as to lead it to failure already in static conditions. Subsequent simulations at lower loads will be performed to determine the ultimate load leading to failure of the coating.

4. EXPERIMENTAL PROCEDURES

The experimental tests on the automotive gear were carried out on the VT250 model axial test machine of the BRT company (Figure **13**) using a gear support fixture and a shank for applying the load. In particular, the gear was forced onto a shaft which was fixed to the support by means of metal clamps, thus creating a friction coupling; the entire gear support system was then rigidly constrained to a plate equipped with a bottom tang, which was then gripped by the gripping devices of the testing machine. Finally, the load was transferred to the gear via a specially shaped top tang to house the cylinder to be forced between two successive teeth. The testing machine used for the tests is of the axial type for both static and dynamic traction and compression tests with a KBM U10M load cell with magnetoresistive transducer; the maximum applicable load is equal to 250 kN in the static phase and 125 kN in the dynamic phase, the maximum frequency is equal to 40 Hz.

With these tests, an attempt was made to determine the fatigue limit of the coating, stressing the gears with a cycle pulsating from zero, sinusoidal in shape and compressive in nature, in a first phase keeping the number of cycles constant and varying the maximum load applied, while in a second phase it is envisaged to carry out tests at constant maximum load in which the number of cycles varies; in this way it is possible to build a diagram linking the number of cycles and the load which lead to failure of the coating, from which to extrapolate its behavior for intermediate conditions with respect to those tested. Finally, the aim of the analysis is to compare the behavior of the coated gear with that of the uncoated gear to verify that the surface coating leads to effective benefits from the point of view of contact fatigue. Up to now tests have been carried out on the coated gear at decreasing loads equal to 15 kN, 10 kN and 5 kN respectively for a number of cycles equal to 50000. As could be expected, given the results of the numerical simulations, for all the loads tested,

(**a**) (**b**)

Figure 13: a) Universal testing machine BRT VT250 and **b**) device designed to apply the fatigue load to the spur gears.

the coating failed on the stressed teeth. There is therefore a first correspondence between the numerical model and experimental evidence; however, further tests are needed to confirm the accuracy of the numerical models set up. In particular, tests were planned with an imposed load lower than those tested (2.5 kN, 1.25 kN and 0.625 kN) to determine the limit load which leads to failure of the surface coating. Once the limit load had been determined, tests were carried out at loads lower than this, varying the number of cycles, thus verifying the accuracy of the numerical model and the predictive analytical model. A further possible evaluation concerns the extent of the damage that occurs on the tooth flank for stress conditions that exceed the resistance limit of the coating; an indication of this parameter can be determined by measuring the area of the print left by the cylinder on the coating. From the tests carried out, it is noted that by increasing the maximum load from 5 kN to 10 kN there is an increase in the frontal area of the impressions left on the tooth. Figures **14-16** show the front and side views of the teeth following the applied load cycles, in which the depth of the impression on the side of the tooth and the damaged surface can be seen.

Finally, two static tests were carried out, with the aim of breaking the entire tooth, applying a maximum load of 70 kN. After both tests, the formation of a through crack was noted which starts under the skin in correspondence with the area where the contact pressure is maximum (Figure **17**). This result is particularly interesting since tooth failure does not occur at the base of the tooth as expected.

5. CONCLUSIONS

The research activity carried out so far has led to the creation of complex numerical models through

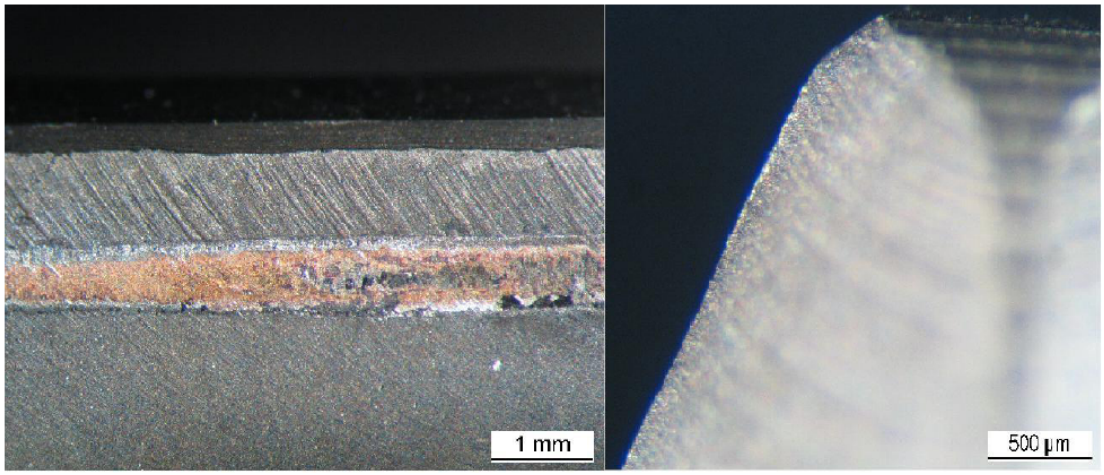

Figure 14: Flank surface of the teeth with applied load 5 kN.

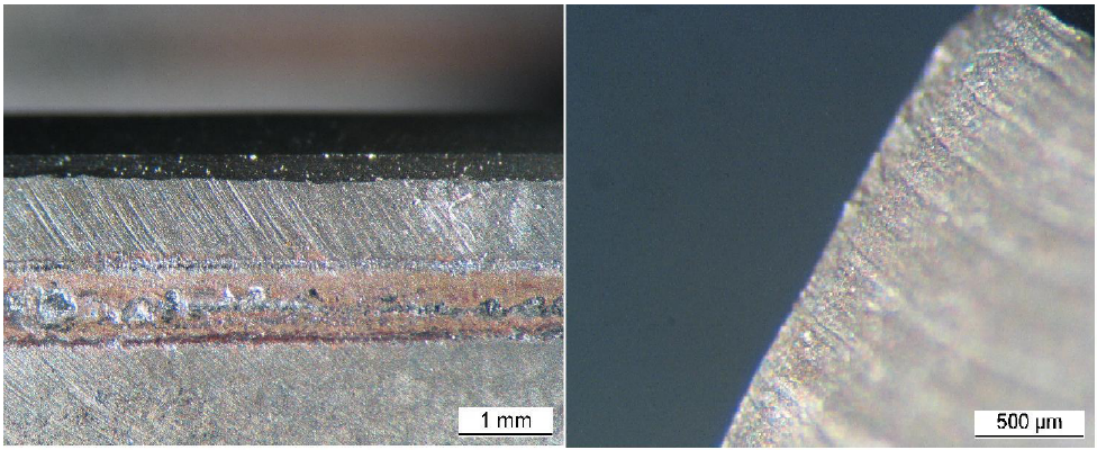

Figure 15: Flank surface of the teeth with applied load 10 kN.

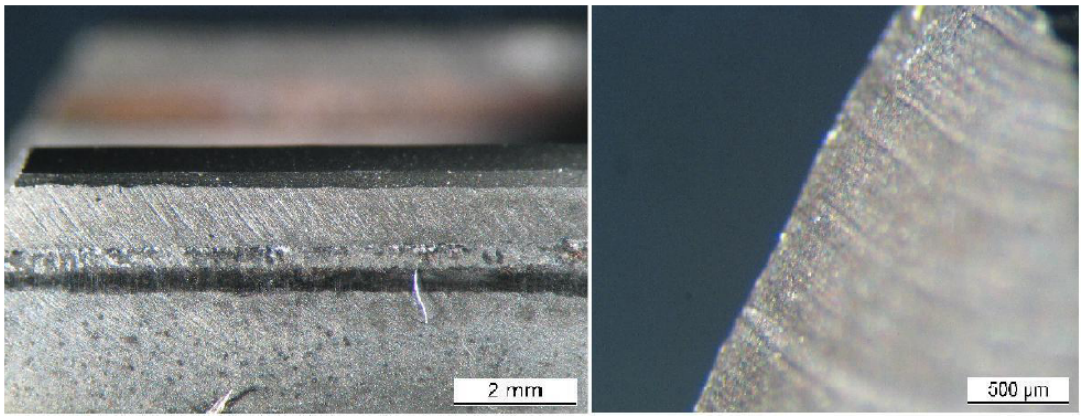

Figure 16: Flank surface of the teeth with applied load 15 kN.

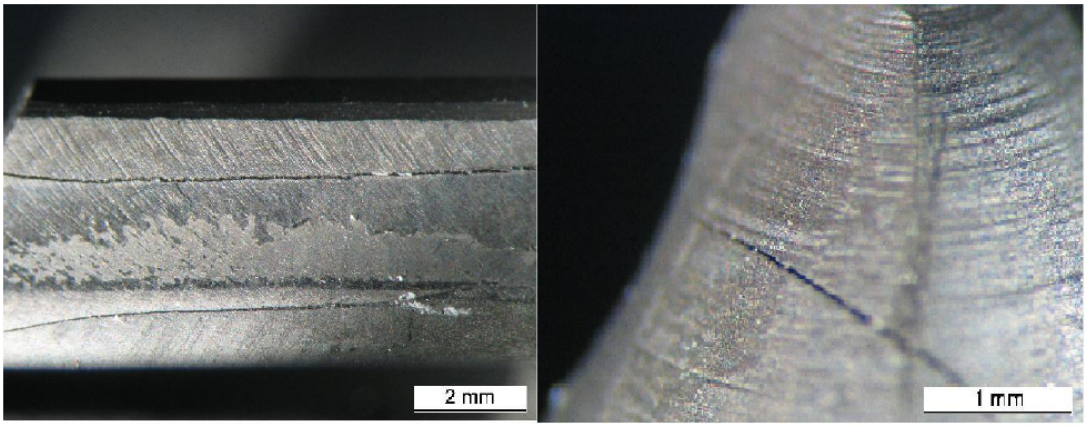

Figure 17: Flank surface of the teeth with applied load 70 kN.

which both the tooth base fatigue and the contact fatigue of spur gears was evaluated. The author applied in this paper the same research method used in previous papers dealing with application in various mechanical engineering fields [22-27]. In the first case, the numerical models have shown how the application of the surface coating leads to effective benefits from the point of view of the propagation of defects, paving the way for the possibility of using different materials for this type of application, compared to the typically used steels. The simulations conducted on coated spur gears made of titanium alloy gave good results, boding well for the use of this and other light alloys, with the resulting advantage in terms of lightness. To complete the research work carried out so far, there is the intention to carry out a campaign of experimental tests, in which the matching conditions between the pinion and the driven gear will be simulated, in order to validate the numerical models created. As far as contact fatigue is concerned, the approach was to set up a campaign of experimental tests and create numerical models that reproduced the conditions in order to verify the applicability of the forecast model chosen. The results obtained cannot yet be said to be sufficient either to carry out an experimental correlation or to confirm the accuracy of the numerical models prepared, for this reason the research work will continue with further experimental tests and associated numerical models, with the aim of determining the limit conditions of use of coated gears, compare coated and uncoated gears and validate the numerical models. Once the accuracy of the FEM models has been confirmed, it will also be possible to study the influence of further parameters such as coating thickness, modulus of elasticity and substrate characteristics.

REFERENCES

[1] Goward GW. Progress in coatings for gas turbine airfoils. Surf Coat Technol 1998; 108-109: 73-9. https://doi.org/10.1016/S0257-8972(98)00667-7

[2] Love CA, Cook RB, Harvey TJ, Dearnley PA, Wood RJK. Diamond like carbon coatings for potential application in biological implants-a review. Tribol Int 2013; 63: 141-50. https://doi.org/10.1016/j.triboint.2012.09.006

[3] Bobzin K, Bagcivan N, Goebbels N, Yilmaz K, Hoehn B-R, Michaeli K, Hochmann M. Lubricated PVD CrAlN and WC/C

coatings for automotive applications. Surf Coat Technol 2009; 204(6-7): 1097-101. https://doi.org/10.1016/j.surfcoat.2009.07.045

[4] Zellner MB, Chen JG. Surface science and electrochemical studies of WC and W2C PVD films as potential electrocatalysts. Catal. Today 2005; 99(3-4): 299-307. https://doi.org/10.1016/j.cattod.2004.10.004

[5] Kumar K, Arul S. Investigation of mechanical properties on nano cuprous oxide coated/uncoated spur gear. IOP Conf Ser: Mater Sci Eng 2020; 954: 012023. https://doi.org/10.1088/1757-899X/954/1/012023

[6] Puchi-Cabrera ES, Staia MH, Lesage J, Gil L, Villalobos-Gutiérrez C, La Barbera-Sosa J, Ochoa-Pérez EA, Le Bourhise E. Fatigue behavior of AA7075-T6 aluminum alloy coated with ZrN by PVD. Int J Fatigue 2008; 30(7): 1220-30. https://doi.org/10.1016/j.ijfatigue.2007.09.001

[7] Arcieri EV, Baragetti S, Borzini E. Bending fatigue behavior of 7075-aluminum alloy. Key Eng Mater 2018; 774: 1-6. https://doi.org/10.4028/www.scientific.net/KEM.774.1

[8] Baragetti S, Arcieri EV. Effects of thin hard film deposition on fatigue strength of AA7075-T6. Proc Inst Mech Eng C: J Mech Eng Sci 2022; 236: 10713-22. https://doi.org/10.1177/0954406220980505

[9] Saini BS, Gupta VK. Effect of WC/C PVD coating on fatigue behaviour of case carburized SAE8620 steel. Surf Coat Technol 2010; 205(2): 511-8. https://doi.org/10.1016/j.surfcoat.2010.07.022

[10] Puchi-Cabrera ES, Staia MH, Ochoa-Pérez EA, Teer DG, Santana-Méndez TT, La Barbera-Sosa JG, Chicot D, Lesage J. Fatigue behavior of a 316L stainless steel coated with a DLC film deposited by PVD magnetron sputter ion plating. Mat Sci Eng A 2010; 527(3): 498-508. https://doi.org/10.1016/j.msea.2009.09.030

[11] Srinivasan N, Bhaskar LK, Kumar R, Baragetti S. Residual stress gradient and relaxation upon fatigue deformation of diamond-like carbon coated aluminum alloy in air and methanol environments. Mater Des 2018; 160: 303-12. https://doi.org/10.1016/j.matdes.2018.09.022

[12] Baragetti S, D'Urso G. Aluminum 6060-T6 friction stir welded butt joints: fatigue resistance with different tools and feed rates. J Mech Sci Technol 2014; 28: 867-77. https://doi.org/10.1007/s12206-013-1152-1

[13] Baragetti S. Corrosion fatigue behaviour of Ti-6Al-4V in methanol environment. Surf Interface Anal 2013; 45: 1654-8. https://doi.org/10.1002/sia.5203

[14] ABAQUS, ABAQUS Documentation, Dassault Systemes, Providence, RI, USA, 2020.

[15] Vergani L. Meccanica dei materiali. Milano: McGraw-Hill; 2005.

[16] Miller KJ. The short crack problem. Fatigue Fract Eng M 1982; 5(3): 223-32. https://doi.org/10.1111/j.1460-2695.1982.tb01250.x

[17] El-Haddad MH, Smith KN, Topper TH. Fatigue crack propagation of short cracks. ASME J Eng Mater Technol 1979; 101: 42-6. https://doi.org/10.1115/1.3443647

[18] Kato M, Deng G., Inoue K, Takatsu N. Evaluation of the strength of carburized spur gear teeth based on fracture mechanics, JSME Int J Ser C 1993; 36(2): 233-240. https://doi.org/10.1299/jsmec1993.36.233

[19] Gelfi M, La Vecchia GM, Lecis N, Troglio S. Relationship between through thickness residual stress of CrN-PVD coatings and fatigue nucleation sites. Surf Coat Technol 2005; 192: 263-8. https://doi.org/10.1016/j.surfcoat.2004.05.032

[20] Shigley JE, Mischke CR, Budynas RG. Progetto e costruzione di macchine. Milano: McGraw-Hill; 2001.

[21] Šraml M, Flašker J. Computational approach to contact fatigue damage initiation analysis of gear teeth flanks. Int J Adv Manuf Technol 2007; 31: 1066-75. https://doi.org/10.1007/s00170-005-0296-2

[22] Baragetti S, Baryshnikov A. Rotary Shouldered Thread Connections: Working Limits Under Combined Static Loading. ASME J Mech Des 2001; 123: 456-63. https://doi.org/10.1115/1.1371476

[23] Baragetti S. A Theoretical Study on Nonlinear Bending of Wires. Meccanica 2006; 41: 443-58. https://doi.org/10.1007/s11012-006-0002-y

[24] Arcieri EV, Baragetti S, Fustinoni M, Lanzini S, Papalia R. Study and modelling of the passenger safety devices of an electric vehicle by finite elements. Procedia Struct Integr 2018; 8: 212-9. https://doi.org/10.1016/j.prostr.2017.12.023

[25] Baragetti S, Arcieri EV. Study on a new mobile anti-terror barrier. Procedia Struct Integr 2019; 24: 91-100. https://doi.org/10.1016/j.prostr.2020.02.008

[26] Baragetti S, Arcieri EV. Study of impact phenomena for the design of a mobile anti-terror barrier: Experiments and finite element analyses. Eng Fail Anal 2020; 113: 104564. https://doi.org/10.1016/j.engfailanal.2020.104564

[27] Arcieri EV, Baragetti S, Božić Ž. Application of design of experiments to foreign object damage on 7075-T6. Procedia Struct Integr 2021; 31: 22–7. https://doi.org/10.1016/j.prostr.2021.03.005

Received on 02-11-2022 Accepted on 15-12-2022 Published on 26-12-2022

DOI: https://doi.org/10.31875/2410-4701.2022.09.08